NANO LETTERS

Letter

pubs.acs.org/NanoLett

Enhanced Endosomal Escape by Light-Fueled Liquid-Metal Transformer

Yue Lu,[†,‡] Yiliang Lin,[§] Zhaowei Chen,[†,‡] Quanyin Hu,[†,‡] Yang Liu,[∥] Shuangjiang Yu,[†,‡,⊥] Wei Gao,[*,#] Michael D. Dickey,[*,§] and Zhen Gu[*,†,‡,▽]

[†]Joint Department of Biomedical Engineering, University of North Carolina at Chapel Hill and North Carolina State University, Raleigh, North Carolina 27695, United States

[‡]Division of Molecular Pharmaceutics and Center for Nanotechnology in Drug Delivery, Eshelman School of Pharmacy, University of North Carolina at Chapel Hill, Chapel Hill, North Carolina 27599, United States

[§]Department of Chemical and Biomolecular Engineering, North Carolina State University, Raleigh, North Carolina 27695, United States

[∥]Department of Materials Science and Engineering, North Carolina State University, Raleigh, North Carolina 27695, United States

[⊥]Key Laboratory of Polymer Ecomaterials, Changchun Institute of Applied Chemistry, Chinese Academy of Sciences, Changchun 130022, China

[#]Department of Textile Engineering, Chemistry and Science, North Carolina State University, Raleigh, North Carolina 27695, United States

[▽]Department of Medicine, University of North Carolina at Chapel Hill, Chapel Hill, North Carolina 27599, United States

Supporting Information

ABSTRACT: Effective endosomal escape remains as the "holy grail" for endocytosis-based intracellular drug delivery. To date, most of the endosomal escape strategies rely on small molecules, cationic polymers, or pore-forming proteins, which are often limited by the systemic toxicity and lack of specificity. We describe here a light-fueled liquid-metal transformer for effective endosomal escape-facilitated cargo delivery via a chemical-mechanical process. The nanoscale transformer can be prepared by a simple approach of sonicating a low-toxicity liquid-metal. When coated with graphene quantum dots (GQDs), the resulting nanospheres demonstrate the ability to absorb and convert photoenergy to drive the simultaneous phase separation and morphological transformation of the inner liquid-metal core. The morphological transformation from nanospheres to hollow nanorods with a remarkable change of aspect ratio can physically disrupt the endosomal membrane to promote endosomal escape of payloads. This metal-based nanotransformer equipped with GQDs provides a new strategy for facilitating effective endosomal escape to achieve spatiotemporally controlled drug delivery with enhanced efficacy.

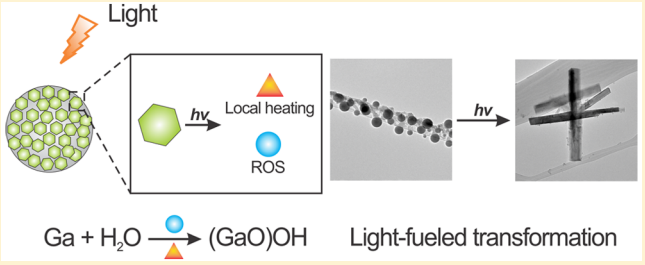

KEYWORDS: *Drug delivery, liquid metal, stimuli-responsive, morphological transformation, endosomal escape*

Limited endosomal escape of cargo molecules during intracellular drug delivery remains as a major challenge in both research and clinical practices.[1−5] To date, most strategies involve small molecules such as chloroquine, cationic polymers such as polyethylenimine (PEI), and bacteria and virus derived pore-forming proteins.[6−8] Despite their efficiency, the broad application and clinical translation of cationic polymer based approaches and protein/peptide dependent strategies are limited due to their systemic toxicity and lack of specificity. More recently, researchers have taken advantage of the photothermal therapy (PTT) and/or photodynamic therapy (PDT) to achieve light-triggered spatialtemporal control over endosome disruption and cargo escape.[9−11] In these strategies, light-generated heat or reactive oxygen species (ROS) could facilitate endosomal escape of cargo molecules. Compared with traditional molecule-based approaches, such external-stimulus controlled systems have several advantages, including the capability of remotely controlling drug release and enhancing spatial precision for minimizing off-target drug release and systemic toxicity.[12,13] Nevertheless, PTT based strategies often suffer from relatively low efficacy due to the limited efficiency of light−heat conversion and the heat loss during the energy transport. In addition, the large thermal excursions make them unsuitable for thermosensitive cargos, including a wide range of protein therapeutics.[14] The effectiveness of PDT based strategies is also restricted by the

Received: October 17, 2016
Revised: March 6, 2017
Published: March 22, 2017

DOI: 10.1021/acs.nanolett.6b04346
Nano Lett. 2017, 17, 2138−2145

short lifetime (below 0.1 ms) and the short action range (usually within 10 to 20 nm) of the ROS.[15] In addition, the ROS generated during PDT could cause oxidation damages to cargo molecules.[16,17]

Herein, we report a light-responsive liquid-metal "nanotransformer" to physically achieve efficient endosomal escape. In our previous demonstration, the eutectic alloy of gallium indium (EGaIn, 75% Ga and 25% In by weight) displays low toxicity and good biocompatibility *in vivo*.[18] Here, we discover that EGaIn-based nanostructures can undergo dramatic morphological transformation in an aqueous environment with appropriate external stimulation, such as heating. To this end, a sonication-based approach is simply applied to bulk EGaIn in an aqueous solution of graphene quantum dots (GQDs) to generate transformable liquid-metal nanoparticles (tNPs).[18−21] The resulting particles appear as uniform nanospheres coated with GQDs. In this formulation, the GQDs not only help control particle size during nanosphere formation but also serve as energy collectors and converters to absorb photoenergy and generate local heat and ROS (Figure 1a,b).[22−24] The locally

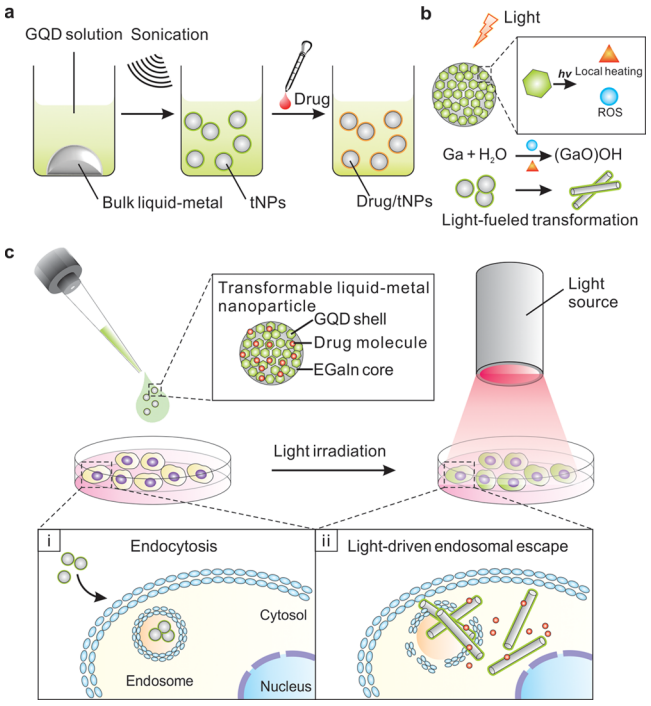

Figure 1. Schematic design of light-fueled liquid-metal transformer. (a) Preparation route of tNPs. (b) GQDs generate localized heating effect and ROS upon light irradiation, enabling the transition of Ga to (GaO)OH, which leads to the morphological transformation from nanospheres to nanorods. (c) GQD-coated tNPs can be used for light-triggered endosomal escape. (i) tNPs enter the cell via endocytosis. (ii) tNPs undergo intracellular morphological transformation to physically disrupt endosomal membrane upon light irradiation.

generated heat and ROS can be consumed by the liquid-metal core to drive the phase separation of the alloy due to the transition of Ga into (GaO)OH, which leads to the subsequent morphological transformation from nanospheres into hollow rods (Figure 1b).[25,26] Such a remarkable transition of aspect ratio can physically disrupt the endosomal membrane to achieve efficient intracellular delivery of cargo molecules (Figure 1c). Additionally, the efficient consumption and elimination of heat and ROS mediated by GQDs can avoid potential and undesired damage to payloads. Collectively, this liquid-metal nanocarrier is transformable in terms of both energy conversion and morphological change. It can efficiently absorb photoenergy and convert the absorbed energy to heat and ROS, which can be consumed by the liquid-metal core to achieve morphological transformation, leading to the physical disruption of cellular structures. This unique energy conversion mechanism could minimize potential photo, thermo, and oxidation damages to cargo molecules. Moreover, with incorporation of fluorescent GQDs, this delivery vehicle can simultaneously serve as imaging agents for spatiotemporal theranostics.[27]

To prepare the tNPs, a small amount of EGaIn (80 μL) was added to a centrifuge tube filled with aqueous solution of GQD. After sonication, the largest particles precipitated within seconds, and the nanoscale colloids were collected from the tube. The resulting tNPs appeared as core−shell structured nanospheres evenly coated with GQDs (Figure S1). These nanoparticles displayed good stability in PBS buffer with no significant change in hydrodynamic diameters for up to 2 weeks (Figure S2). To be noted, GQDs behaved like a surfactant during the sonication to help control the particle size (Figure S3). Like the GQDs, the tNPs also exhibited the excitation-dependent emission behavior (Figure S4).

To study the light-triggered morphological transformation, we irradiated tNPs with light at a power density of 100 mW cm^{-2}. Considering the efficiency of tissue penetration depth, we chose 635 nm as the irradiation wavelength.[28] Transmission electron microscopy (TEM) imaging helped to visualize the morphological change of tNP with up to 20 min of light (Figure 2b). We classified the different morphologies observed during this process into four stages (designated M1, M2, M3, and M4). Conversion of M1 stage to M2 stage appeared within the first 5 min of light irradiation. We spotted the initial sign of phase separation at this stage in which nanofragments grew from the spherical nanoparticles (M1). During the following 10 min, these nanofragments gradually assembled into oval-shaped nanosheets (M3). The nanosheets then transformed into the rod-like nanostructures (M4) with the continuous light irradiation. The calculation and statistical analysis of large quantities of TEM data also revealed a remarkable increase in the aspect ratio of nanostructures (Figure 2a).

To reveal the nature behind this light-induced morphological change, we monitored the whole transformation process using energy dispersive X-ray spectroscopy (EDS) mapping (Figures S5 and 2c). Previous to the light irradiation, the tNPs appeared as core−shell structured nanospheres with alloy cores and surface coating of GQDs. The colocalization of Ga and O within the nanostructures observed in stages M2 to M4 indicated that the shape transformation of tNPs could be a result of the oxidation of Ga. More importantly, higher GQD signals were found associated with the nanofragments and nanosheets composed of metal oxides, suggesting a GQD-mediated morphological transformation mechanism. Of note, a dramatic structure shift from nanosheets (M3) into nanorods (M4) was observed. A closer examination revealed that the nanosheets could rapidly roll up to form nanorods with light irradiation (Figure 2d). The architecture of the formed rod-shaped structures was further validated via electron tomography based 3D reconstruction (Figure 2e). The reconstructed model clearly shows the hollow tubular structures, while the remaining ultrasmall spheres were proven to be indium by EDS (Figure 2e,c). To further identify the role of GQDs in the shape

DOI: 10.1021/acs.nanolett.6b04346
Nano Lett. 2017, 17, 2138−2145

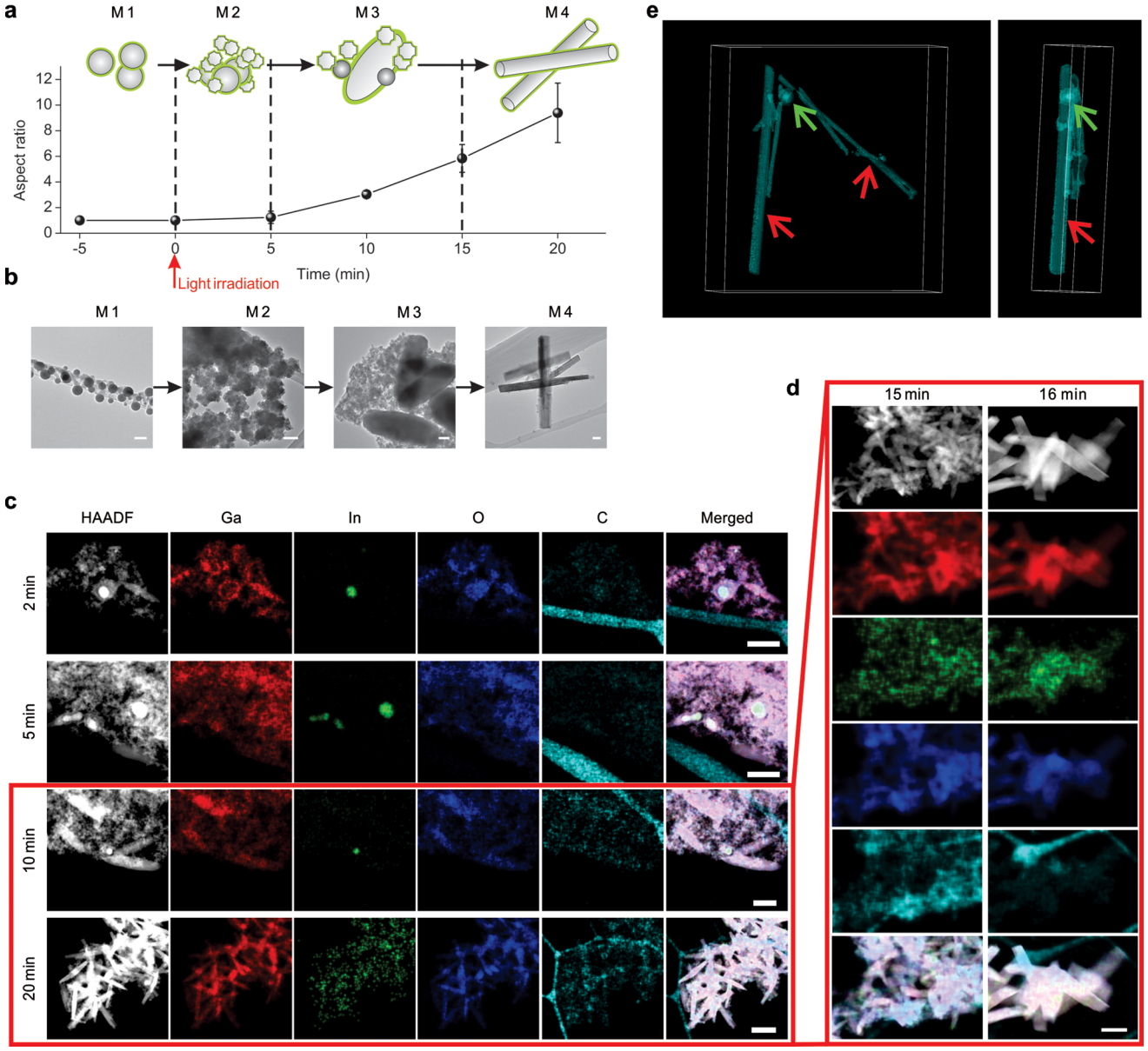

Figure 2. Light-induced morphological transformation. (a) Schematic changes of aspect ratio of the tNPs over light irradiation time. Gray spheres in M2 and M3 represent remaining nanospheres. Error bars indicate SD (n = 100). (b) Representative TEM images of tNPs after different light irradiation time. Scale bars: 100 nm. (c) EDS mapping of tNPs after different irradiation duration. Scale bars: 200 nm (2, 5, and 10 min); 500 nm (20 min). (d) Crystalline nanosheets rolled-up into nanorods. Scale bar: 500 nm. (e) Three-dimensional reconstruction of nanostructures formed after phase separation using electron tomography. Red arrows show hollow nanorods, and green arrows show the remaining nanosphere.

transformation, we irradiated EGaIn nanoparticles with light at the same intensity, but without GQD coating, subsequently no sign of morphological change was observed (Figure S6).

Evidenced by the X-ray powder diffraction (XRD) analysis, the nanorods were composed of (GaO)OH, which is a preferred form of gallium oxide in water,[29] while the existence of an amorphous bump agreed well with the formation of intermediate nanofragments observed during TEM imaging (Figures 3a and 2b,c). We hypothesized that the light-induced phase separation and the simultaneous formation of (GaO)OH nanorods could be attributed to the reaction between gallium and the surrounding water powered by the photothermal and photodynamic effects of GQDs. With the continuous consumption of gallium into (GaO)OH nanorods, the remaining metal is no longer at the eutectic composition, and therefore, the indium precipitates, forming spherical nanoparticles to minimize the surface energy (Figure 2c). In other words, dealloying occurs during the shape transformation of the liquid metal nanoparticles. In this system, GQD serves as an energy convertor and effectively converted photoenergy to local heating and ROS generation, providing the necessary conditions for oxidizing gallium. It is suggested that the GQDs here not only provide a stimulus for the transformation but also facilitate the reaction without affecting the surrounding environments significantly.

To test our hypothesis that heating induces the transformation and dealloying of liquid metal NPs, we first sonicated liquid metal alloy while controlling temperature (Figure 3b). Nanorods formed at elevated temperature (near boiling) and proved to be (GaO)OH crystals according to the XRD

DOI: 10.1021/acs.nanolett.6b04346
Nano Lett. 2017, 17, 2138−2145

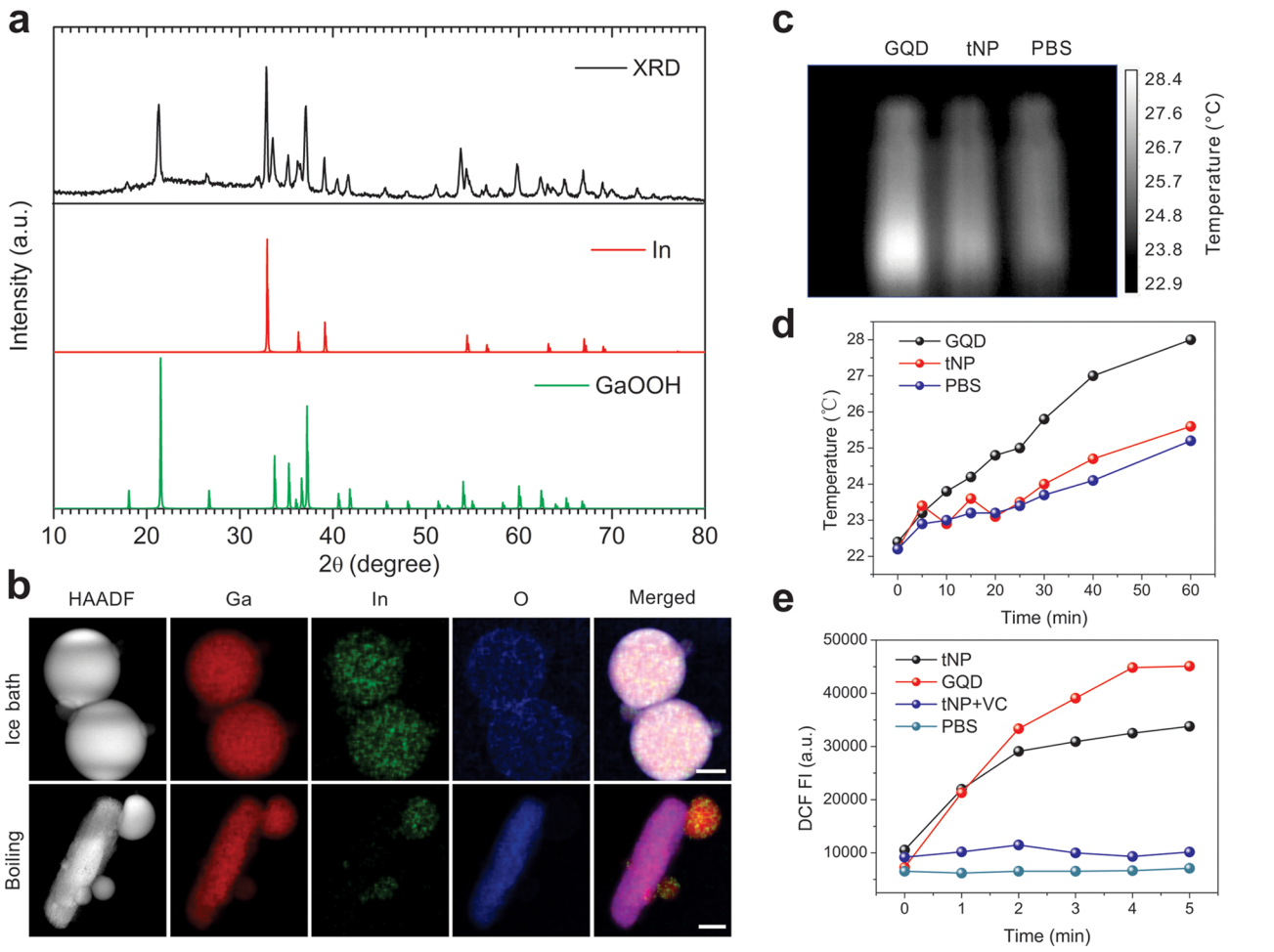

Figure 3. Mechanism of light-driven phase separation. (a) XRD spectrum of light-irradiated tNPs. (b) EDS mapping of EGaIn nanoparticles sonicated under different temperatures. Scale bars: 50 nm. (c) FLIR image of GDQ solution, tNP suspension, and PBS buffer after light irradiation for 1 h. (d) Temperature increases of GQD solution, tNP suspension, and PBS buffer upon light irradiation. (e) Changes of ROS concentrations over light irradiation time.

spectrum (Figure S7). However, when the sonication was performed in an ice bath to prevent the temperature increase, the alloy broke into NPs due to the acoustic cavitation.[19] EDS clearly showed that the gallium and indium maps overlap in these particles, and thus, there was no dealloying. In both cases, ultrasonication generated sufficient ROS to guarantee a supply of oxidizer, suggesting that heating is a necessary condition for phase separation and (GaO)OH formation. We then monitored the temperature change of tNP solution during light irradiation. As displayed in Figure 3c,d, an obvious temperature increase occurred in the GQD buffer upon light irradiation. Interestingly, no significant difference in temperature increase was observed between tNP solution and DI water, suggesting efficient heat transfer and consumption within the tNPs. Similar trends were observed with GQD and tNP solutions irradiated by light in a 37 °C environment (Figure S8).

Next, we investigated the light-triggered ROS generation capability of tNPs utilizing 2′,7′-dichlorofluorescin diacetate (DCFH-DA), a sensitive ROS indicator that could be rapidly oxidized by ROS into fluorescent dichlorofluorescein (DCF).[30] As displayed in Figure 3e, both GQD and tNP efficiently generate ROS with exposure to light. The significantly lower ROS level generated by tNP relative to GQD (at the same GQD concentration as the GQD solution) could be attributed to the ROS consumption during the oxidation of gallium. Additionally, the ROS generation of tNP could be effectively quenched by the ROS scavenger vitamin C (VC).[28] Taken together, upon exposure to light, GQDs could generate local heating and ROS to power the reaction between gallium and water and to propel the phase separation, thus achieving remote and precise control over the morphological transformation of tNPs.

We hypothesized that if the morphological transformation occurred intracellularly, it could physically disrupt the endosomal membrane to facilitate endosomal escape. The cellular uptake of tNP displayed an energy-dependent manner, and tNP mainly entered HeLa cells via caveolin-mediated endocytosis and macropinocytosis (Figure S9). To assess the detailed intracellular behaviors of tNPs, we quantified their intracellular ROS production upon light exposure. As shown in Figure 4a, tNPs could efficiently generate ROS intracellularly with light irradiation, and this photodynamic process could be easily inhibited by preincubating cells with VC. Next, the cytotoxicity of both GQDs and tNPs toward HeLa cells was evaluated by 3-(4,5-dimethylthiazol-2-yl)-2,5-diphenyltetrazolium bromide (MTT) assay (Figure 4b).[31] GQDs displayed significant cytotoxicity with light irradiation, as expected, while tNPs only showed moderate cytotoxicity at the same GQD dose. In other words, the heat and ROS produced by the GQDs could

DOI: 10.1021/acs.nanolett.6b04346
Nano Lett. 2017, 17, 2138−2145

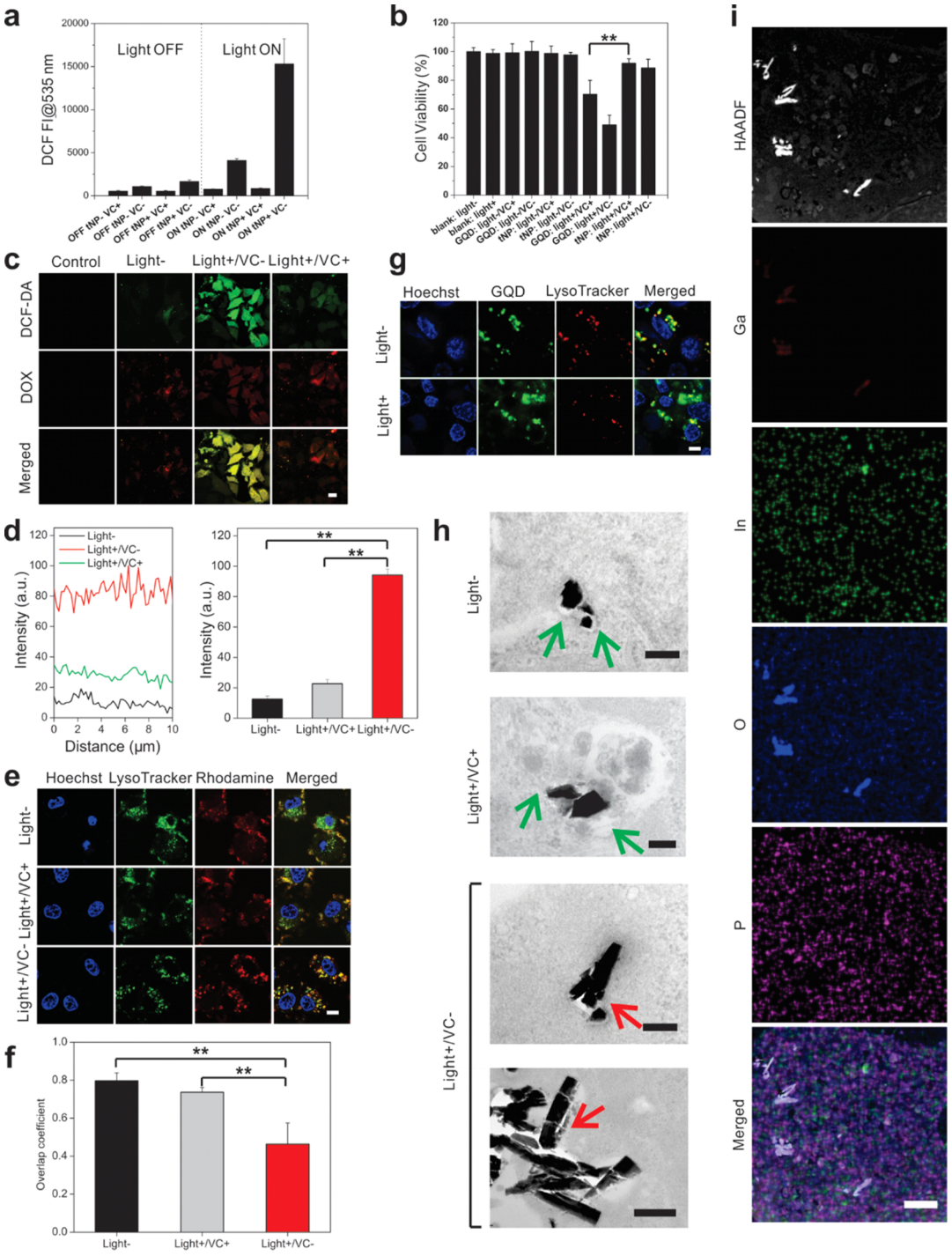

Figure 4. Intracellular behavior. (a) Quantification of intracellular ROS concentration. Error bars indicate SD (n = 4). (b) MTT results suggested that LM core effectively consumed heat and ROS generated by GQD to avoid potential cytotoxicity. Error bars indicate SD (n = 4). $^{**}P < 0.01$ (two-tailed Student's t-test). (c) Intracellular ROS generation (visualized by the fluorescence signal of ROS indicator DCF-DA) and physically driven DOX release. Scale bar: 20 μm. (d) Typical fluorescence intensity of Dox at the nuclei and statistical analysis. Error bars indicate SD (n = 20). (e) Promoted intracellular protein delivery. Model protein BSA was labeled with Rhodamine. Scale bar: 10 μm. (f) Colocalization of Rho-BSA and endosome quantified by the overlap coefficient. Error bars indicate SD (n = 4). (g) tNP for live cell imaging. Scale bar: 10 μM. (h) Representative TEM images that show the intracellular behavior of tNPs without and with light irradiation. Green arrows show intact endosome membrane, while red arrows show disrupted membrane. Scale bars: 200 nm (Light−, Light+/VC+, and Light+/VC−, upper) and 500 nm (Light+/VC−, lower). (i) Representative EDS mapping of intracellular phase separation and morphological transformation. Scale bar: 2 μm.

be readily consumed by the LM core for morphological transformation, which could be appealing for delivering cargo molecules that are vulnerable to heat or oxidation.

Next, we chose two model molecules to test the light-triggered endosomal escape: small molecule doxorubicin (Dox),[32] a broad-spectrum chemotherapeutic, and bovine serum albumin (BSA). Dox was loaded onto GQDs via $\pi-\pi$ stack interaction (designated Dox/tNP),[33] while rhodamine-labeled BSA (Rho-BSA) was directly anchored onto the surface of LM core through a polyethylene glycol (PEG)-based linker

DOI: 10.1021/acs.nanolett.6b04346
Nano Lett. 2017, 17, 2138−2145

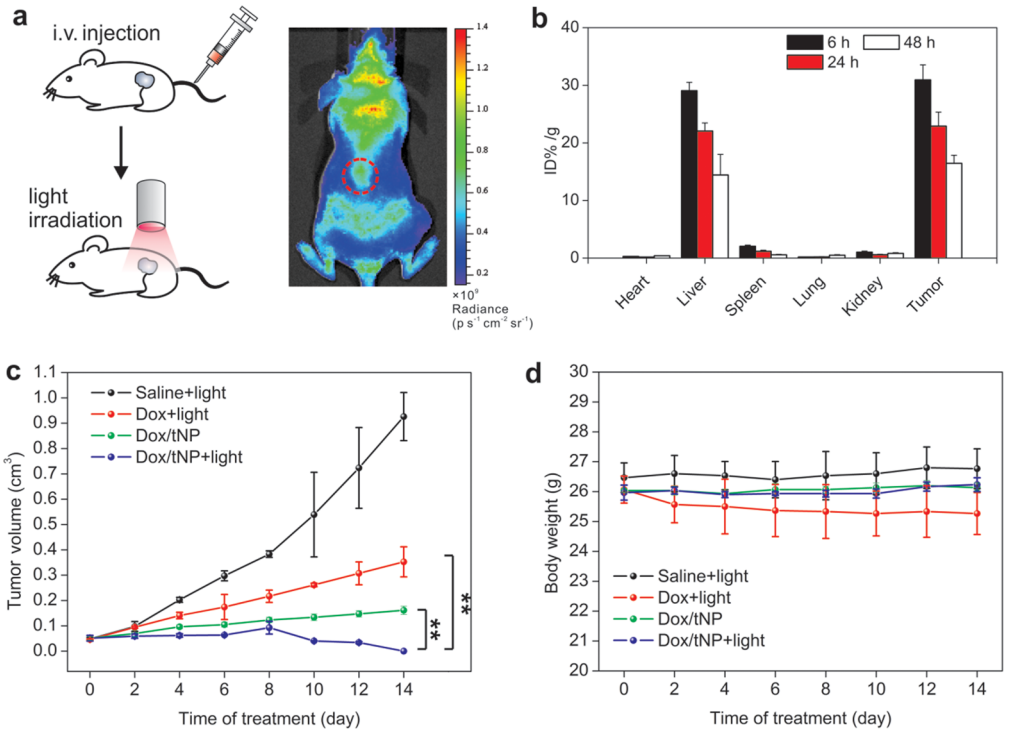

Figure 5. Liquid-metal transformer for light-controlled *in vivo* drug release. (a) Scheme of antitumor efficacy evaluation: HeLa tumor-bearing nude mice were first intravenously injected with saline, free Dox solution, and Dox/*t*NP, respectively. For light treatment groups, the tumor sites were irradiated with light after each intravenous injection. tNP can also be used for live imaging of diseased tissue (circled in red). (b) Time-dependent biodistribution of Dox/tNP in HeLa tumor-bearing nude mice at 6, 24, and 48 h after intravenous injection of Dox/tNP determined by gallium concentration. Error bars indicate SD (n = 4). (c) The HeLa tumor growth curves after intravenous injection of different formulations of Dox at a dose of 2 mg kg^{-1}. Error bars indicate SD (n = 4). $^{**}P < 0.01$ (two-tailed Student's t-test). (d) The body weight variation of HeLa tumor-bearing mice during treatment. Error bars indicate SD (n = 4).

(designated BSA/tNP). Promoted endosomal escape of both molecules were observed with light irradiation (Figure 4c–f). To verify the enhanced Dox release, we monitored the fluorescence signal of Dox at the nuclei site, and remarkable stronger Dox signal was found in cells irradiated with light (Figure 4d). The promoted endosomal escape of Rho-BSA was quantified by the overlap coefficient of the fluorescence signals of rhodamine and Lysotracker Green. A significant decrease of the overlap coefficient in the cells with light treatment suggested a tNP-facilitated endosomal escape (Figure 4f). To validate that the enhanced endosomal escape was a result of the tNP transformation, HeLa cells were preincubated with ROS scavenger VC. With VC treatment, lower fluorescence signals for both molecules were observed in the cytosol. Moreover, tNP was fluorescent and thus can simultaneously serve as imaging agents (Figure 4g). We also evaluated the anticancer capability of Dox/tNP toward HeLa cells using the MTT assay (Figure S10). Although Dox/tNP without light treatment only displayed a moderate cell killing effect after 24 h incubation (IC_{50} = 1.25 mg L^{-1}, Dox concentration), the combination of Dox/tNP and photoirradiation generated a 2.6-fold higher cytotoxicity (IC_{50} = 0.35 mg L^{-1}, Dox concentration).

To further confirm the physical disruption of endosomal membrane caused by the light-fueled transformation of tNPs, we visualized the intracellular behaviors of tNPs by TEM imaging (Figures 4h and S11). Without light exposure, tNPs fused with each other within the endosome, a process that was established and described in our previous work.[18] The endosomal membrane remained intact during the fusion process. With light treatment, a clear shape transformation was also observed intracellularly. At some sites, remaining membrane fragments were observed together with nanorods breaking out of the endosomes, while in other locations, the endosomal membrane was fully disrupted by the noticeable morphological change and volume increase of tNP. The disruption of the endosomal membrane was directly related with the shape transformation sites, instead of "isotropic disruption". VC was once again employed as a transformation inhibitor, and in this group, no significant morphological change was observed, and the endosome membrane remained intact. EDS results further confirmed the morphological transition happened intracellularly (Figure 4i).

Next, we evaluated the anticancer efficacy of our system *in vivo* utilizing the female J:NU nude mice bearing with cervical cancer tumor. First, the single-dose, acute toxicity of tNP to mice was investigated by identifying the maximum tolerated dose (MTD).[34] The estimated MTD of tNP was determined to be 750 mg kg^{-1}, suggesting low acute toxicity, which highly favored its *in vivo* applications. To evaluate the tumor targeting capability of Dox/tNP, HeLa tumor-bearing nude mice were sacrificed at 6, 24, and 48 h after intravenous injection of Dox/tNP for tissue collection, and the time-dependent biodistribution of Dox/tNP was further quantified by ICP–MS. Significant tumor accumulations were observed within a short time period (Figure 5b). The antitumor efficacy of Dox/tNP was then assessed. After successive intravenous administration of different formulations including saline, free Dox solution, and Dox/tNP, the tumor sites were irradiated with red light (wavelength 635 nm) with a power density of 100 mW cm^{-2} (Figure 5a). Among these formulations, Dox/tNP accompanied

DOI: 10.1021/acs.nanolett.6b04346
Nano Lett. 2017, 17, 2138–2145

by the phototreatment showed the most potent inhibition efficacy toward HeLa tumor growth with tumors completely eliminated at day 14 (Figure 5c). More importantly, a significant difference in tumor growth inhibition between the group that received Dox/tNP together with light irradiation and the control group with mice that received Dox/tNP injection at the same dose but without light irradiation was observed. Moreover, no significant change of mice body weights was observed during the treatment of Dox/tNP injection and photoirradiation, and no noticeable sign of side effects was revealed (Figure 5d).

In summary, we have developed a light-fueled liquid-metal transformer for enhanced endosomal escape. The formulation can be easily formed in an environmental-friendly aqueous solution via facile sonication with the presence of GQDs. The resulting GQD-coated nanospheres are capable of absorbing and converting the photoenergy to drive the phase separation and the simultaneous morphological transformation of their metallic cores. This light-fueled dramatic shape change and volume increase lead to the physical disruption of the endosomal membrane, facilitating the endosomal escape of cargo molecules to realize controlled drug release. Considering the unique energy-conversion feature of this system, it could potentially serve as a promising tool for delivery of thermo or oxidization sensitive cargoes such as protein therapeutics. The light-controlled effective disruption of cellular structure achieved by this liquid-metal transformer provide new opportunities for precisely controlled spatiotemporal release of cargo molecules or complexes that require additional assistance for endosomal escape, for example, nucleic acids for gene delivery and genome editing.[4,35−37] Moreover, considering the photophysical properties of GQDs and the energy transfer between GQD and liquid-metal, new applications of this platform are expected to be exploited for bioimaging and optical devices.[38−41]

■ ASSOCIATED CONTENT

Supporting Information

The Supporting Information is available free of charge on the ACS Publications website at DOI: 10.1021/acs.nanolett.6b04346.

Experimental details and Figures S1−S11 (PDF)

■ AUTHOR INFORMATION

Corresponding Authors

*E-mail: zgu@email.unc.edu (Z.G.).
*E-mail: mddickey@ncsu.edu (M.D.D.).
*E-mail: wgao5@ncsu.edu (W.G.).

ORCID

Zhen Gu: 0000-0003-2947-4456

Author Contributions

Yue Lu and Yiliang Lin contributed equally to this work. The manuscript was written through contributions of all authors. All authors have given approval to the final version of the manuscript.

Notes

The authors declare no competing financial interest.

■ ACKNOWLEDGMENTS

This work was supported by the Sloan Research Fellowship (to Z.G.) and the NSF MRSEC DMR-1121107 (to M.D.D.). We acknowledge the use of the Analytical Instrumentation Facility (AIF) and the Cellular and Molecular Imaging Facility (CMIF) at North Carolina State University. We acknowledge Victoria Madden and Valerie Lapham for their assistance in the TEM imaging of biological specimens.

■ REFERENCES

(1) Mitragotri, S.; Burke, P. A.; Langer, R. *Nat. Rev. Drug Discovery* **2014**, *13*, 655−672.
(2) Whitehead, K. A.; Langer, R.; Anderson, D. G. *Nat. Rev. Drug Discovery* **2009**, *8*, 129−138.
(3) Varkouhi, A. K.; Scholte, M.; Storm, G.; Haisma, H. J. *J. Controlled Release* **2011**, *151*, 220−228.
(4) Peer, D.; Karp, J. M.; Hong, S.; Farokhzad, O. C.; Margalit, R.; Langer, R. *Nat. Nanotechnol.* **2007**, *2*, 751−760.
(5) Chow, E. K.; Zhang, X.-Q.; Chen, M.; Lam, R.; Robinson, E.; Huang, H.; Schaffer, D.; Osawa, E.; Goga, A.; Ho, D. *Sci. Transl. Med.* **2011**, *3*, 73ra21−73ra21.
(6) Mellman, I.; Fuchs, R.; Helenius, A. *Annu. Rev. Biochem.* **1986**, *55*, 663−700.
(7) Boussif, O.; Lezoualc'h, F.; Zanta, M. A.; Mergny, M. D.; Scherman, D.; Demeneix, B.; Behr, J.-P. *Proc. Natl. Acad. Sci. U. S. A.* **1995**, *92*, 7297−7301.
(8) Kay, M. A.; Glorioso, J. C.; Naldini, L. *Nat. Med.* **2001**, *7*, 33−40.
(9) Dreaden, E. C.; Mackey, M. A.; Huang, X.; Kang, B.; El-Sayed, M. A. *Chem. Soc. Rev.* **2011**, *40*, 3391−3404.
(10) Berg, K.; Selbo, P. K.; Prasmickaite, L.; Tjelle, T. E.; Sandvig, K.; Moan, J.; Gaudernack, G.; Fodstad, Ø.; Kjølsrud, S.; Anholt, H. *Cancer Res.* **1999**, *59*, 1180−1183.
(11) Kim, H.; Lee, D.; Kim, J.; Kim, T.-i.; Kim, W. J. *ACS Nano* **2013**, *7*, 6735−6746.
(12) Timko, B. P.; Arruebo, M.; Shankarappa, S. A.; McAlvin, J. B.; Okonkwo, O. S.; Mizrahi, B.; Stefanescu, C. F.; Gomez, L.; Zhu, J.; Zhu, A.; Santamaria, J.; Langer, R.; Kohane, D. S. *Proc. Natl. Acad. Sci. U. S. A.* **2014**, *111*, 1349−1354.
(13) Rwei, A. Y.; Wang, W.; Kohane, D. S. *Nano Today* **2015**, *10*, 451−467.
(14) Frokjaer, S.; Otzen, D. E. *Nat. Rev. Drug Discovery* **2005**, *4*, 298−306.
(15) Yuan, Y.; Liu, J.; Liu, B. *Angew. Chem., Int. Ed.* **2014**, *53*, 7163−7168.
(16) Yu, B. P. *Physiol. Rev.* **1994**, *74*, 139−162.
(17) Wiseman, H.; Halliwell, B. *Biochem. J.* **1996**, *313*, 17.
(18) Lu, Y.; Hu, Q.; Lin, Y.; Pacardo, D. B.; Wang, C.; Sun, W.; Ligler, F. S.; Dickey, M. D.; Gu, Z. *Nat. Commun.* **2015**, *6*, 10066.
(19) Hohman, J. N.; Kim, M.; Wadsworth, G. A.; Bednar, H. R.; Jiang, J.; LeThai, M. A.; Weiss, P. S. *Nano Lett.* **2011**, *11*, 5104−5110.
(20) Boley, J. W.; White, E. L.; Kramer, R. K. *Adv. Mater.* **2015**, *27*, 2270−2270.
(21) Khan, M. R.; Eaker, C. B.; Bowden, E. F.; Dickey, M. D. *Proc. Natl. Acad. Sci. U. S. A.* **2014**, *111*, 14047−14051.
(22) Bonaccorso, F.; Colombo, L.; Yu, G.; Stoller, M.; Tozzini, V.; Ferrari, A. C.; Ruoff, R. S.; Pellegrini, V. *Science* **2015**, *347*, 1246501.
(23) Ge, J.; Lan, M.; Zhou, B.; Liu, W.; Guo, L.; Wang, H.; Jia, Q.; Niu, G.; Huang, X.; Zhou, H. *Nat. Commun.* **2014**, *5*, 4596.
(24) Burke, A.; Ding, X.; Singh, R.; Kraft, R. A.; Levi-Polyachenko, N.; Rylander, M. N.; Szot, C.; Buchanan, C.; Whitney, J.; Fisher, J. *Proc. Natl. Acad. Sci. U. S. A.* **2009**, *106*, 12897−12902.
(25) Métraux, G. S.; Cao, Y. C.; Jin, R.; Mirkin, C. A. *Nano Lett.* **2003**, *3*, 519−522.
(26) Sun, Y.; Mayers, B.; Xia, Y. *Adv. Mater.* **2003**, *15*, 641−646.
(27) Peng, J.; Gao, W.; Gupta, B. K.; Liu, Z.; Romero-Aburto, R.; Ge, L.; Song, L.; Alemany, L. B.; Zhan, X.; Gao, G. *Nano Lett.* **2012**, *12*, 844−849.
(28) Qian, C.; Yu, J.; Chen, Y.; Hu, Q.; Xiao, X.; Sun, W.; Wang, C.; Feng, P.; Shen, Q. D.; Gu, Z. *Adv. Mater.* **2016**, *28*, 3313−3320.
(29) Khan, M. R.; Trlica, C.; So, J.-H.; Valeri, M.; Dickey, M. D. *ACS Appl. Mater. Interfaces* **2014**, *6*, 22467−22473.

DOI: 10.1021/acs.nanolett.6b04346
Nano Lett. 2017, 17, 2138−2145

(30) Shim, M. S.; Xia, Y. *Angew. Chem., Int. Ed.* **2013**, *52*, 6926−6929.
(31) van Meerloo, J.; Kaspers, G. J.; Cloos, J. *Methods Mol. Biol.* **2011**, *731*, 237−245.
(32) Tacar, O.; Sriamornsak, P.; Dass, C. R. *J. Pharm. Pharmacol.* **2013**, *65*, 157−170.
(33) Yang, K.; Feng, L.; Shi, X.; Liu, Z. *Chem. Soc. Rev.* **2013**, *42*, 530−547.
(34) Yu, T.; Greish, K.; McGill, L. D.; Ray, A.; Ghandehari, H. *ACS Nano* **2012**, *6*, 2289−2301.
(35) Langer, R.; Tirrell, D. A. *Nature* **2004**, *428*, 487−492.
(36) LaVan, D. A.; McGuire, T.; Langer, R. *Nat. Biotechnol.* **2003**, *21*, 1184−1191.
(37) Yin, H.; Song, C.-Q.; Dorkin, J. R.; Zhu, L. J.; Li, Y.; Wu, Q.; Park, A.; Yang, J.; Suresh, S.; Bizhanova, A.; Gupta, A.; Bolukbasi, M. F.; Walsh, S.; Bogorad, R. L.; Gao, G.; Weng, Z.; Dong, Y.; Koteliansky, V.; Wolfe, S. A.; Langer, R.; Xue, W.; Anderson, D. G. *Nat. Biotechnol.* **2016**, *34*, 328−333.
(38) Rosi, N. L.; Mirkin, C. A. *Chem. Rev.* **2005**, *105*, 1547−1562.
(39) Michalet, X.; Pinaud, F.; Bentolila, L.; Tsay, J.; Doose, S.; Li, J.; Sundaresan, G.; Wu, A.; Gambhir, S.; Weiss, S. *Science* **2005**, *307*, 538−544.
(40) Kroutvar, M.; Ducommun, Y.; Heiss, D.; Bichler, M.; Schuh, D.; Abstreiter, G.; Finley, J. J. *Nature* **2004**, *432*, 81−84.
(41) Lu, Y.; Aimetti, A. A.; Langer, R.; Gu, Z. *Nat. Rev. Mater.* **2016**, *1*, 16075.

DOI: 10.1021/acs.nanolett.6b04346
Nano Lett. 2017, 17, 2138−2145